Published in final edited form as:
Magn Reson Med. 2011 November ; 66(5): 1312–1326. doi:10.1002/mrm.22925.

T_1-corrected fat quantification using chemical shift-based water/fat separation: application to skeletal muscle

Dimitrios C. Karampinos[1], **Huzanzhou Yu**[2], **Ann Shimakawa**[2], **Thomas M. Link**[1], and **Sharmila Majumdar**[1]

[1]Department of Radiology and Biomedical Imaging, University of California, San Francisco, San Francisco, CA, USA

[2]Global Applied Science Laboratory, GE Healthcare, Menlo Park, CA, USA

Abstract

Chemical shift based water/fat separation, like iterative decomposition of water and fat with echo asymmetry and least-squares estimation (IDEAL), has been proposed for quantifying intermuscular adipose tissue (IMAT). An important confounding factor in IDEAL-based IMAT quantification is the large difference in T_1 between muscle and fat, which can cause significant overestimation in the fat fraction. This T_1 bias effect is usually reduced by employing small flip angles. T_1-correction can be performed by employing at least two different flip angles and fitting for T_1 of water and fat. In the present work, a novel approach for the water/fat separation problem in a dual flip angle experiment is introduced and a new approach for the selection of the two flip angles, labeled as the unequal small flip angle approach, is developed, aiming to improve the noise efficiency of the T_1-correction step relative to existing approaches. It is shown that the use of flip angles, selected such the muscle water signal is assumed to be T_1-independent for the first flip angle and the fat signal is assumed to be T_1-independent for the second flip angle, has superior noise performance to the use of equal small flip angles (no T_1 estimation required) and the use of large flip angles (T_1 estimation required).

Keywords

water/fat separation; fat quantification; intermuscular adipose tissue

INTRODUCTION

Muscular fat has been associated with different metabolic abnormalities including obesity and insulin resistance (1–3). The non-invasive assessment of skeletal muscle lipids would be an important alternative to the highly invasive muscle biopsies, and it would allow analysis of muscles, which are less accessible to biopsy. Different MRI techniques have been proposed for assessing the different compartments of muscular fat (4). Specifically, skeletal muscle fat includes intramyocellular lipids (IMCLs) and extramyocellular lipids (EMCLs). IMCLs are located within muscle fibers in the form of cytosolic triacyglycerols. EMCLs represent adipocytes located between muscle fibers and muscle fiber bundles and can be divided into two compartments: intermuscular fat and intramuscular fat. Intramuscular fat corresponds to adipocytes present between muscle fibers and muscle fiber bundles within individual muscles. Intermuscular fat corresponds to adipocytes present between muscle

Corresponding Author Address: Dimitrios Karampinos, Suite 203, 1700 4th Street, San Francisco, CA 94158, USA, phone: +1-415-514-9662, fax: +1-415-514-9656, dimitrios.karampinos@ucsf.edu.

groups and beneath the muscle fascia. According to the literature, the superposition of intermuscular fat and intramuscular fat that is visible on T_1-weighted images constitutes the intermuscular adipose tissue (IMAT) compartment (3). Volume localized spectroscopy and low resolution spectroscopic imaging techniques have been widely used for the quantification of IMCLs and EMCLs (5,6). However, the spatial distribution of IMAT cannot be assessed accurately by low resolution spectroscopic imaging techniques and requires high spatial resolution imaging (7).

Because of the high resolution requirement, the distribution and the total area/volume of IMAT have been traditionally assessed using T_1-weighted imaging (8). However, quantification of IMAT based on T_1-weighted imaging is limited by residual partial volume effects and requires effective and accurate segmentation procedures (9). Some alternative techniques that have been proposed for measuring total intramuscular lipid content combine fat selective excitation with gradient echo imaging (7,10) or high spatial resolution spectroscopic imaging (11–13). Fat selective gradient echo imaging requires a reliable reference signal and fat selective high spatial resolution spectroscopic imaging suffers from prolonged scan times. Chemical-shift based water/fat separation (14–16) has recently received considerable attention for fat quantification in different body parts (17,18). Therefore, chemical shift-based water-fat separation techniques could be used to derive quantitative IMAT fat fraction maps. Three-point Dixon techniques (14) and iterative decomposition of water and fat with echo asymmetry and least-squares estimation (IDEAL) (19) have been recently implemented to measure fat content in dystrophic skeletal muscle (20,21).

In order to get accurate fat content measurements with quantitative IDEAL multiple confounding factors have to be taken into consideration. Specifically, the spectral complexity of fat (17,18), the T_2* decay (17,22) and the T_1 bias effects (23) have to be considered. Multi-peak T_2* IDEAL based on at least 6 time-point measurements has been proposed to overcome the two first confounding factors (18). Regarding the T_1 bias effect, the large T_1 difference (values at 3 T) between muscle (1500 ms) and fat (360 ms) can cause a significant overestimation in the fat fraction (17,23). The acquisition of data at small flip angle (SFA) has been proposed to reduce T_1 weighting (17,23) and the acquisition of data at two flip angles (dual flip angle-DFA) or multiple flip angles has been used to correct for T_1 weighting (23–25). However, the SFA method can be limited by low SNR and a method that corrects for T_1 effects based on multiple flip angles suffers from prolonged scan times (23,25). At least two flip angles are required to fit for the proton-density weighted signal and the T_1 of both the water and fat compartments. Therefore, the dual flip angle (DFA) acquisition can correct for T_1 bias effects at the cost of increasing the minimum scan time, but the introduction of additional unknowns increases the signal model complexity and may degrade the noise performance of the fat fraction estimation (23,25). This problem of noise degradation in the fat fraction estimation of the DFA acquisition has been assessed in the case of tissues with small T_1 differences between water and fat compartments (i.e. liver) (23,25), but it has not been studied in the case of tissues with large T_1 differences between water and fat compartments (i.e. skeletal muscle).

In the present work, the problem of T_1-unbiased estimation of fat fraction from dual flip angle multi-peak T_2* IDEAL data is separated into a water/fat separation problem and a T_1-correction problem. In terms of the water/fat separation problem, a new approach, labeled as joint fieldmap estimation IDEAL, is introduced for the implementation of IDEAL algorithm on dual flip angle data. Specifically, it is investigated whether performing a joint water/fat separation at the two employed flip angles improves the noise performance of the water signal, fat signal and fat fraction estimates relative to the traditional approach of performing the water/fat separation separately at every flip angle. In terms of the T_1-correction problem,

a new approach, labeled as the unequal small flip angle approach, is introduced in the selection of the employed flip angles. Specifically, it is investigated whether the use of two small unequal flip angles, selected such the water signal is assumed to be T_1-independent for the first flip angle and the fat signal is assumed to be T_1-independent for the second flip angle, provides superior noise performance to the use of the same small flip angle twice (no T_1 estimation required) and the use of two unequal large flip angles (T_1 estimation required). Therefore, a thorough comparison of the accuracy and noise performance of the different water/fat separation approaches and the different T_1 bias reduction and correction procedures is presented in the context of IMAT quantification, using numerical simulations and water/fat phantom measurements. Finally, the noise performance of the different approaches is qualitatively compared in the calf muscle region of a healthy volunteer.

THEORY

Signal model

The multi-peak T_2* IDEAL signal model (18) can be enhanced by using a multi-peak fat spectrum that takes into account the T_1 weighting of the individual fat peaks. If a_p is the proton density-weighted relative amplitude of the p-th fat peak (p=1,…,P, such that $\sum_{p=1}^{P} a_p = 1$), and $a_{p,cor}$ is the T_1-weighted relative amplitude of the p-th fat peak, the signal model of a voxel containing water (ρ_w) and fat (ρ_f) in a spoiled gradient echo (SPGR) experiment with echo time t, repetition time TR and flip angle α can be written as:

$$S(t,\alpha)=\left[\rho_w \frac{(1-\exp(-TR/T_{1w}))\sin(\alpha)}{1-\exp(-TR/T_{1w})\cos(\alpha)}+\rho_f\left(\sum_{p=1}^{P} a_p \frac{(1-\exp(-TR/T_{1fp}))\sin(\alpha)}{1-\exp(-TR/T_{1fp})\cos(\alpha)}\right)\sum_{p=1}^{P} a_{p,cor}(\alpha)\exp(j2\pi\Delta f_p t)\right]\exp(j2\pi\psi t)\exp(-t/T_2^*) \quad [1]$$

where Δf_p is the resonance frequency difference of the p-th peak with respect to water, ψ is the local fieldmap frequency offset and T_{1w} and T_{1fp} are the T_1 relaxation times of water and p-th fat peak, respectively. It should be noticed that Eq. [1] assumes that T_2* values of water and all fat peaks are equal.

The T_1-weighted relative amplitudes of the fat peaks are in general flip angle dependent:

$$a_{p,cor}(\alpha)=\frac{a_p \frac{(1-\exp(-TR/T_{1fp}))\sin(\alpha)}{1-\exp(-TR/T_{1fp})\cos(\alpha)}}{\sum_{p=1}^{P} a_p \frac{(1-\exp(-TR/T_{1fp}))\sin(\alpha)}{1-\exp(-TR/T_{1fp})\cos(\alpha)}} \quad [2]$$

and such that $\sum_{p=1}^{P} a_{p,cor}(\alpha)=1$.

The problem of extracting the fat fraction from the above measurements can be considered a two-step problem. First, the T_1-weighted water and fat signals are separated by solving the following water/fat separation problem:

$$S(t,\alpha)=\left[M_w(\alpha)+M_f(\alpha)\sum_{p=1}^{P} a_{p,cor}(\alpha)\exp(j2\pi\Delta f_p t)\right]\exp(j2\pi\psi t)\exp(-t/T_2^*) \quad [3]$$

Second, the proton density weighted water and fat signals can be extracted based on the SPGR signal expressions:

$$M_w(\alpha)=\rho_w\frac{(1-\exp(-TR/T_{1w}))\sin(\alpha)}{1-\exp(-TR/T_{1w})\cos(\alpha)} \quad [4]$$

$$M_f(\alpha)=\rho_f\left(\sum_{p=1}^{P}a_p\frac{(1-\exp(-TR/T_{1fp}))\sin(\alpha)}{1-\exp(-TR/T_{1fp})\cos(\alpha)}\right) \quad [5]$$

The fitting of the T_1 of the different fat peaks would require in general the acquisition of a very high number of flip angles. A spectroscopy-based precalibration of the T_1 of the different fat peaks would require the repetition of the spectroscopy experiment with multiple TRs. Instead, it is proposed to assume that for the range of the employed flip angles the effect of modeling the T_1 of different fat peaks equal to the T_1 of the dominant fat peak ($T_{1fp}=T_{1f}$) can be neglected. This simplifying assumption leads to the result that $a_{p,cor}(\alpha) = a_p$ and Eq. [5] becomes:

$$M_f(\alpha)=\rho_f\frac{(1-\exp(-TR/T_{1fp}))\sin(\alpha)}{1-\exp(-TR/T_{1fp})\cos(\alpha)} \quad [6]$$

T_1-bias minimization/correction

The extraction of the proton-density weighted water and fat signal values, based on Eqs. [4] and [6], requires in general the estimation of T_1 of water and fat. However, Eqs. [4] and [6] can be roughly considered T_1-independent at flip angles sufficiently smaller than the Ernst flip angles of water and fat, respectively. Therefore, T_1-bias minimization/correction can be performed following three approaches, when two flip angles are collected in a dual flip angle IDEAL experiment:

Equal small flip angles (ESFA) approach—First, the two flip angles can be selected to be equal and substantially smaller than the Ernst flip angles of both water and fat, such that the T_1 weighting in both Eqs. [4] and [6] can be neglected. This first method of minimizing the T_1-bias effect is labeled in the present study as equal small flip angles (ESFA) approach and it is equivalent to the small flip angle approach with two averages proposed in previous studies (17,23,26,27).

Specifically, if the two flip angles are equal $\alpha_1 = \alpha_2 = \alpha$ and have been selected such that $M_w(\alpha) \approx \rho_w\alpha$ and $M_f(\alpha) \approx \rho_f\alpha$, there is no T_1-correction step required since the fat fraction is

$$\eta=\frac{M_f(\alpha)}{M_f(\alpha)+M_w(\alpha)}\approx\frac{\rho_f}{\rho_f+\rho_w} \quad [7]$$

Therefore, the ESFA approach has two unknowns $M_w(\alpha_1)$, $M_f(\alpha_1)$.

Unequal large flip angles (ULFA) approach—Second, in the general case that both flip angles are not sufficiently smaller than the Ernst flip angles of water and fat, T_1 estimation of both compartments is required. This second method of correcting the T_1-bias effect is labeled in the present study as unequal large flip angles (ULFA) approach it is equivalent to the dual flip angle approach proposed in previous studies (23,25).

Specifically, in the most general case that the two flip angles have been selected such that neither of the water nor the fat SPGR signal expressions is T_1-independent, the proton-density weighted water and fat signals can be computed based on Eqs. [4] and [6]:

$$\rho_w = \frac{M_w(\alpha_1)M_w(\alpha_2)(\cos(\alpha_1) - \cos(\alpha_2))}{M_w(\alpha_1)\sin(\alpha_2)(\cos(\alpha_1) - 1) - M_w(\alpha_2)\sin(\alpha_1)(\cos(\alpha_2) - 1)} \quad [8]$$

$$\rho_f = \frac{M_f(\alpha_1)M_f(\alpha_2)(\cos(\alpha_1) - \cos(\alpha_2))}{M_f(\alpha_1)\sin(\alpha_2)(\cos(\alpha_1) - 1) - M_f(\alpha_2)\sin(\alpha_1)(\cos(\alpha_2) - 1)} \quad [9]$$

Therefore, the ULFA approach has four unknowns $M_w(\alpha_1)$, $M_f(\alpha_1)$, $M_w(\alpha_2)$, $M_f(\alpha_2)$.

Unequal small flip angles (USFA) approach—Third, the two flip angles can be selected to be unequal and such that one (α_1) is sufficiently smaller than the Ernst flip angle of water and the other one (α_2) is sufficiently smaller than the Ernst flip angle of fat. Because T_{1f} is typically shorter than T_{1w}, $\alpha_1 < \alpha_2$. Then, Eq. [6] can be approximately considered T_1-independent for both flip angles and Eq. [4] can be considered T_1-independent only for the smaller flip angle (α_1).

Specifically, if the flip angles are not equal and have been selected such that $M_w(\alpha_1) \approx \rho_w\alpha_1$ and $M_f(\alpha_2) \approx \rho_f\alpha_2$ (which means that also $M_f(\alpha_1) \approx \rho_f\alpha_1$), then the proton density weighted water signal can be computed from the first flip angle (α_1) data and the proton density weighted fat signal can be computed from both flip angles (α_1 and α_2) data in the least squares sense:

$$\rho_w \approx \frac{M_w(\alpha_1)}{\alpha_1} \quad [10]$$

$$\rho_f \approx \frac{\alpha_1 M_f(\alpha_1) + \alpha_2 M_f(\alpha_2)}{\alpha_1^2 + \alpha_2^2} \quad [11]$$

Therefore, the USFA approach has three unknowns $M_w(\alpha_1)$, $M_f(\alpha_1)$, $M_w(\alpha_2)$, since $M_f(\alpha_2) = (\alpha_2 / \alpha_1) M_f(\alpha_1)$.

Water/fat separation

The water/fat separation problem involves in general the extraction of the T_1-weighted water and fat signals $M_w(\alpha_1)$, $M_f(\alpha_1)$ and $M_w(\alpha_2)$, $M_f(\alpha_2)$ at two flip angles based on the multi-echo source signals $\{S(t_1, \alpha_1),\ldots, S(t_6, \alpha_1)\}$ and $\{S(t_1, \alpha_2),\ldots, S(t_6, \alpha_2)\}$, respectively. In the present work, the following two options are investigated for the water/fat separation problem at two flip angles described by Eq. [3].

Independent fieldmap estimation (IFE) IDEAL—The water/fat separation step can be performed independently for the two different flip angles employing the multi-peak T_2* IDEAL algorithm (18) separately for each flip angle. The fieldmap is estimated based on a region growing scheme for every flip angle separately as in (28). This approach is labeled as independent fieldmap estimation IDEAL.

Joint fieldmap estimation (JFE) IDEAL—The fieldmap ψ and T_2* values are common unknowns for the independent fieldmap estimation IDEAL problem at both flip angles. Therefore, it is proposed to use the T_1-weighted multi-echo source signals at both flip angles to jointly estimate the T_1-weighted water, fat signals at both flip angles. The approach of joint estimation of the T_1-weighted water, fat signals at both flip angles, is labeled as joint fieldmap estimation IDEAL. Appendix A1 presents the matrix formulation of the multi-peak T_2* IDEAL problem with joint fieldmap estimation at two flip angles extending the formulation presented by Yu et al. (18,22). The matrix formulation of the joint fieldmap estimation IDEAL can also be modified to take into account the constraints imposed by the employed T_1 bias minimization/correction approach (see Appendix A1). The joint fieldmap estimation IDEAL is performed in two steps: Independent fieldmap estimation IDEAL is performed first to extract initial estimates for the water/fat separation problem at the two flip angles separately. The derived field map ψ and T_2* values from the implementation of independent fieldmap estimation IDEAL at the two different flip angles are averaged and introduced as initial estimates of the joint fieldmap estimation IDEAL problem.

The magnitude discrimination approach is applied to the T_1-weighted water and fat signals after the water/fat separation step and before the T_1-correction step in order to remove noise bias effects at high and low fat fractions as previously proposed by Liu et al. (23).

Selection of flip angles

If the T_1 values of water and fat are constant and known and there are no variations of the actual flip angle across the field-of-view relative to the nominal flip angle, the problem of T_1-correction becomes straightforward as ρ_w and ρ_w can be calculated directly from Eq. [4] and Eq. [6] for a given flip angle and estimated M_w and M_f. In the present work, it is assumed that T_1 of water is unknown and varying in the range between T_{1wmin} and T_{1wmax} and the T_1 of fat is considered to be unknown and constant. The maximum T_1-induced fat fraction bias occurs for a nominal fat fraction approximately equal to 50%. Therefore, the flip angles for the above two approaches that do not correct but minimize the T_1 bias effect (namely the ESFA and USFA approaches) are selected such that the T_1-induced fat fraction bias is minimized for a nominal fat fraction of 50%.

Equal small flip angles (ESFA)—As the employed flip angles increase, the result of Eq. [7] is not any more valid and the T_1 bias effect increases. At very small flip angles, the bias effect is minimized but the SNR for both the water and fat signal is low, degrading the noise properties of the fat fraction measurement. A common approach to select the small flip angle is to allow a T_1 biased fat fraction η at a nominal fat fraction f. The optimal small flip angle resulting in T_1-biased fat fraction η for a nominal fat fraction f is described by the equation:

$$\cos(\alpha)=\frac{(1-\exp(-TR/T_{1f}))f(1-\eta)-(1-\exp(-TR/T_{1w}))\eta(1-f)}{(1-\exp(-TR/T_{1f}))\exp(-TR/T_{1w})f(1-\eta)-(1-\exp(-TR/T_{1w}))\exp(-TR/T_{1f})\eta(1-f)} \quad [12]$$

The results of Eq. [12] are equivalent to the ones presented by Hines et al (29) but the final mathematical expression (Eq. [12]) is simpler in the present derivation than the one in (29).

The maximum T_1-induced fat fraction bias occurs for a nominal fat fraction f approximately equal to 50% and for T_1 equal to T_{1wmax}. Therefore, the flip angle of the ESFA approach is selected such that the worst case of T_1-induced fat fraction when f=50% and for T_1=T_{1wmax} is equal to a given fat fraction bias (in our case set to 2%). The flip angle of the ESFA approach is then derived by Eq. [12] with T_{1w}=T_{1wmax}, η=52% and f=50%. For the parameters used in the simulations and the phantom experiments (TR=40ms, T_{1wmin}=500 ms, T_{1wmax}=2000 ms, T_{1f}=360 ms), the optimal flip angle for the ESFA approach is 3.7°.

Unequal large flip angles (ULFA)—The ULFA approach totally removes the T_1 bias and the optimal flip angles are derived such that the noise performance of the T_1-correction procedure is maximized. The derivation of the flip angles that maximize the noise performance for the ULFA approach requires the performance of numerical simulations of both the water/fat separation and the T_1-correction step. Numerical simulations are performed using 6 echoes, TE_{min}=1.27 ms, ΔTE=0.65 ms, TR=40 ms, the multi-peak fat spectrum of the phantom excluding the glycerin peak (see below), T_{1w}=1500 ms, T_{1f}=360 ms, for fat fraction values between 0% and 100% and flip angles in the range between 1° and 50°. Gaussian noise is added in quadrature to the simulated data assuming SNR=50 for the fat signal at the flip angle of the ESFA approach and 1000 repetitions are performed. The optimal flip angles are computed so that the mean variance of the estimated fat fraction over the entire nominal fat fraction range (0 to 100%) is minimized. Figure 1a shows the isocontours of the mean variance of the fat fraction as a function of the two employed flip angles. Point A (Fig. 1a) corresponds to the optimal flip angles (7.2° and 42°) for the ULFA approach (for the parameters used in the simulations and phantom experiments).

Unequal small flip angles (USFA)—The optimal flip angles of the USFA approach are computed, similar to the ESFA approach, such that the SNR is maximized with the constraint that the worst case fat fraction bias does not exceed a given threshold. The isocontours of the fat fraction bias as a function of the two employed flip angles are plotted in Figure 1b for T_{1wmin} and T_{1wmax}. The optimal flip angles pair is selected as the maximum flip angles pair, to maximize SNR, for which the maximum absolute bias is Df=2% for both T_{1wmin} and T_{1wmax}. Specifically, the two flip angles are selected so that the T_1-induced bias is equal to $-$Df=$-$2% for T_{1wmin} and +Df=+2% for T_{1wmax}. Point B (Fig. 1b) corresponds to the optimal flip angles (5.7° and 11.6°) for the USFA approach (for the parameters used in the simulations and phantom experiments).

MATERIALS AND METHODS

Numerical simulations

Numerical simulations are performed to examine the noise performance of the following alternatives for T_1 unbiased estimation of fat fraction:

- T_1 bias correction/minimization step: three options are examined including ESFA, ULFA and USFA approaches.
- Water/fat separation step: two options are examined including independent fieldmap estimation IDEAL and joint fieldmap estimation IDEAL.

The simulation parameters are 6 echoes, TE_{min}=1.27 ms, ΔTE=0.65 ms, TR=40 ms (values for 3 T experiments), the employed flip angles are equal to the optimal flip angles for the ESFA, ULFA and USFA approaches. The multi-peak fat spectrum measured in the phantom excluding the glycerin peak (see below) is employed. Gaussian noise is added in quadrature to the simulated data assuming SNR=50 for the fat signal at the flip angle of the ESFA approach. 1000 repetitions are generated for every fat fraction. The data is then analyzed using all the alternatives for the water/fat separation step and the T_1 bias correction/minimization step (six options in total). The mean and standard deviation of fat fraction are computed after extreme outlier removal. A fat fraction value is considered to be an extreme outlier if its distance to the interquartile interval (i.e. interval between the 25^{th} and 75^{th} percentiles) exceeds three times the length of the interquartile interval.

Central to any approach that estimates or corrects for T_1 weighting in SPGR experiments is the sensitivity of the approach to absolute flip angle variations. Absolute flip angle variations can occur due to calibration errors and transmit B_1 inhomogeneities. The effect of

absolute flip angle variations is tested for all three T_1 bias correction/minimization approaches using numerical simulations.

Phantom experiment

A water/fat phantom with varying fat fraction and T_{1w} was built to validate the simulations results. A spin-echo experiment with multiple repetition times (0.25 s, 0.5 s, 0.75 s, 1 s, 1.5 s and 2s) was performed in five 55-ml water vials with variable concentration of $CuSO_4$ (1 mM, 1.25mM, 1.67 mM, 2.5 mM and 5 mM) to measure the dependence of the T_1 of a Cu-doped aqueous solution with the Cu concentration. The derived calibration curve was $T_1=1.51/C$ where T_1 is in s and C in mM.

A water/fat phantom with Cu doping was constructed containing 28 16-ml plastic vials with fat content by weight (2.5%, 5.0%, 7.5%, 10%, 12.5%, 15% and 17%) and Cu concentration (0.75 mM, 1.0 mM, 1.5 mM and 3 mM). The varying fat fraction was achieved by diluting with a 20% Intralipid fat emulsion (Baxter Healthcare Corporation, Deerfield, IL, USA) and the varying Cu concentration was achieved by diluting with a 20 mM $CuSO_4$ stock solution. The labeled fat fraction of Intralipid is 20% soybean oil by weight and 1.2% glycerin by weight. The proton density weighted fat and glycerin fraction of Intralipid in the phantom vials was computed taking into account the formulas in (30) and was equal to (2.7%, 5.4%, 8.1%, 10.8%, 13.6%, 16.3% and 18.6%). The 28 vials of the water/fat phantom with Cu doping were arranged such that 4 rows (corresponding to the different concentration of Cu) and 7 columns (corresponding to the different fat fractions) were formed, as shown in Fig. 2.

MRI measurements

Precalibration of fat spectrum—Single voxel magnetic resonance spectroscopy measurements (PRESS sequence, TE=28 ms, TR=6000 ms, 10×10×20 mm^3 voxel, 64 averages, no water suppression) were performed on a separate vial with 20% fat Intralipid without any further dilution. 8 different peaks were identified in frequency locations [−69 148 257 327 353 404 442 493] Hz at 3 T. The peak at 148 Hz corresponded to the glycerin and the rest of the peaks corresponded to the soybean oil. The area of the peaks was corrected for T_2 effects resulting in relative peak areas [7.7 5.1 5.6 9.3 6.9 3.9 56 5.5] %. Single voxel spectroscopy experiments were also performed on separate vials with 20% and 10% fat Intralipid and no Cu doping with different TR values (TR= 1080, 2000, 3000, 4000 and 5000 and 6000 ms) to evaluate the dependence of T_1 of fat with fat content in the phantom. The results showed small variation of T_1 of the methylene fat peak with the fat content. Specifically, the saturation recovery fitting results gave a T_1 of the methylene fat peak equal to 356 ms and 374 ms for the phantom vials with fat fraction 10% and 20%, respectively.

For the *in vivo* data, the precalibrated fat spectrum from (31) was used. Single voxel spectroscopy experiments were also performed on regions with different IMAT content with different TR values similarly to the phantom in order to evaluate the dependence of T_1 of fat with fat content *in vivo*. The results showed again small variation of T_1 of the methylene fat peak with the fat content (the T_1 of the methylene fat peak varied between 430 ms and 500 ms).

IDEAL measurements—A quadrature knee coil was used to scan the variable fat fraction/T_1 phantom and the middle-calf muscle region of a healthy female volunteer (age 30) on a 3 T Signa HDx system (GE Healthcare, Waukesha, WI, USA). An investigational version of 6-point IDEAL in a 3D SPGR sequence with a monopolar readout gradient was used. The imaging parameters in the phantom experiments were: TR=40 ms, TE_{min}=1.27 ms, ΔTE=0.65 ms, 2 echoes per TR (3 shots), flip angles= [3.7°, 3.7°, 5.7°, 7.2°, 11.6°, 42°],

bandwidth=83.5 kHz, FOV=16×16 cm^2, acquisition matrix size 128×64 (reconstruction matrix 256×256), 6 slices with 4 mm slice thickness. The phantom IDEAL experiment was repeated 32 times to assess noise performance as in (26,32). The total scan time for the phantom experiment was 4 hours and 7 minutes (there was a dead time equal to 30 ms after every repetition of every flip angle). The imaging parameters in the *in vivo* experiments were: TR=10 ms, TE_{min}=1.09 ms, ΔTE=0.58 ms, 2 echoes per TR (3 shots), flip angles= [2.7°, 2.7°, 3.3°, 5.4°, 6.0°, 31°], bandwidth=83.5 kHz, FOV=20×20 cm^2, acquisition matrix size 128×64 (reconstruction matrix 256×256), 6 slices with 4 mm slice thickness. The *in vivo* IDEAL experiment was repeated 10 times to assess noise performance. The total scan time for the *in vivo* experiment was 20 minutes (there was a dead time equal to 8 ms after every repetition of every flip angle). In the *in vivo* experiment, a shorter TR was used than in the phantom experiment to minimize the total scan time. The flip angles of the *in vivo* experiment were selected based on the same flip angle selection arguments as in the phantom experiment but with TR=10 ms.

RESULTS

Numerical simulations

Figure 3 shows a plot of fat fraction bias at 50% fat fraction for the 3 employed T_1-correction approaches as a function of T_{1w} with no absolute flip angle variation and with absolute flip angle increase equal to 30% of the nominal value. The results show only a relatively small increase in the T_1 induced fat fraction bias in the presence of absolute flip angle variations for all three employed T_1 bias correction/minimization approaches. This result can be explained by the theoretical analysis of the three approaches. In the case of the small equal flip angles approach, the effect of absolute flip angle variations cancels out for the flip angle range that Eq. [7] is valid. However, in the presence of absolute flip angle variations that result in higher flip angle than the nominal one, the deviation from the small flip angle approximation increases and the T_1 induced fat fraction bias increases (ESFA approach in Fig. 4). As it has been shown by Liu et al. (23), in the case of the unequal large flip angles approach, the effect of absolute flip angle variations totally cancels out in the fat fraction estimates for flip angles sufficiently small such that $\sin(\alpha) \approx \alpha$ and $\cos(\alpha) \approx 1 - \alpha^2/2$ (as shown in Appendix A2). However, in the presence of absolute flip angle variations that result in higher flip angles than the nominal ones, such that the results of Appendix A2 are not valid, the T_1 induced fat fraction bias increases (ULFA approach in Fig. 3). In the case of the unequal small flip angles approach, the effect of absolute flip angle variations also cancels out for the flip angle range that Eqs. [10] and [11] are valid. However, in the presence of absolute flip angle variations that result in higher flip angles than the nominal ones, the deviation from the approximations of Eqs. [10] and [11] increases and the T_1 induced fat fraction bias increases (USFA approach in Fig. 3). The results in Fig. 3 show that for all 3 approaches (ESFA, USFA and ULFA), the increase of the T_1 induced fat fraction bias does not overcome 1% even in the presence of absolute flip angle variations that result in flip angles higher by 30% than the nominal ones.

Figure 4 shows the comparison of the of noise performance for the 6 methods under study on the simulation data. The first and second column of Fig. 4 show the standard deviation results for the water and fat signal, respectively. In the case of independent fieldmap estimation IDEAL, the USFA approach shows reduced standard deviation in the water and fat signal when compared to ESFA and ULFA approaches. Specifically, a significant reduction in the standard deviation of the fat signal is observed by using the USFA approach at small fat fractions compared to ESFA and ULFA approaches. Furthermore, the joint fieldmap estimation IDEAL method reduces overall the standard deviation in the estimation of water signal and fat signal compared to the independent fieldmap estimation IDEAL method for all three T_1 bias correction/minimization approaches. Specifically, the joint

fieldmap estimation IDEAL method considerably improves the noise performance in the estimation of the water signal for the ULFA approach and the USFA approach, compared with independent fieldmap estimation IDEAL approach. Similarly, joint fieldmap estimation IDEAL shows much superior noise performance in the estimation of the fat signal for the ULFA approach, compared with independent fieldmap estimation IDEAL approach. The third column of Fig. 4 shows the standard deviation results for the fat fraction. Since the fat fraction is a non-linear function of the water and fat signal and the water and fat signal estimates are dependent, the fat fraction standard deviation results are a little less intuitive than the water and fat signal standard deviation results. In the case of independent fieldmap estimation IDEAL, the standard deviation in the fat fraction is lower with the USFA approach than with the ESFA and ULFA approaches but only for fat fractions between 0 and 35%. However, in the case of joint fieldmap estimation IDEAL the noise performance of the USFA approach in the estimation of the fat fraction at moderate fat fraction values is much improved compared to the independent fieldmap estimation IDEAL and ends up being superior to the ESFA and ULFA approaches. Therefore, based on the simulation results in Fig. 4, the USFA approach combined with joint fieldmap estimation IDEAL shows the lowest standard deviations for the water signal, the fat signal and the fat fraction in the entire range of fat fraction values.

Phantom measurements

Figure 5 shows the T_1 bias effect over the phantom fat fraction range for three different concentrations of Cu. For a given flip angle, as the concentration of Cu decreases, the T_1 of water increases and the T_1 difference between the water and fat compartments also increases leading to a stronger T_1 bias effect (the Cu concentration increases from left to right in Fig. 5). For a given Cu concentration, as the flip angle increases, a stronger T_1 bias in fat fraction is also observed (the different symbols correspond to different flip angle data in Fig. 5). Figure 6 shows the T_1 corrected fat fraction estimates over the phantom fat fraction range for the 0.75 mM concentration in Cu vials. All three T_1 bias correction/minimization approaches (ESFA, ULFA, and USFA) reduce the T_1 bias effect and result in fat fraction values very close to the nominal ones. The fat fraction values have been computed with and without the magnitude discrimination approach (23) to remove noise bias at the small fat fraction range. The estimated fat fraction results at the low true fat fraction in Fig. 6 show that the noise bias correction is essential for all three T_1 bias correction/minimization approaches (ESFA, ULFA and USFA) and all two water/fat separation approaches (independent fieldmap estimation IDEAL and joint fieldmap estimation IDEAL).

Figures 7, 8 and 9 show the standard deviation results for the proton density weighted water signal, the proton density weighted fat signal and the fat fraction respectively employing the 6 alternatives under study on the phantom data. In the fat fraction range and T_1 range of the phantom, the USFA approach has the lowest standard deviation for the water signal, the ULFA approach has a moderate standard deviation for the water signal, and the ESFA has the highest standard deviation for the water signal (Fig. 7). The joint fieldmap estimation IDEAL approach improves the noise performance of the water signal estimates relative to the independent fieldmap estimation IDEAL approach for all three T_1 bias correction/ minimization approaches (ESFA, ULFA, and USFA) in the fat fraction range between 10% and 17%. Furthermore, in the fat fraction range and T_1 range of the phantom, the USFA approach has the lowest standard deviation for the fat signal, the ULFA approach has a moderate standard deviation for the fat signal, and the ESFA has the highest standard deviation for the fat signal (Fig. 8). The joint fieldmap estimation IDEAL approach does not alter significantly the noise performance of the fat signal estimates relative to the independent fieldmap estimation IDEAL approach for all three T_1 bias correction/ minimization approaches (ESFA, ULFA, and USFA). Finally, in the fat fraction range and

T_1 range of the phantom, the USFA approach has the lowest standard deviation for the fat fraction, the ULFA approach has a moderate standard deviation for the fat fraction, and the ESFA has the highest standard deviation for the fat fraction (Fig. 9). Specifically, Fig. 9 shows that the USFA approach leads to a decrease in the standard deviation of fat fraction up to 50% compared with the ESFA approach. In summary, the phantom measurements show a superior noise performance in water, fat and fat fraction estimation for the USFA approach when compared to the ESFA and ULFA approaches in the fat fraction range and T_1 range of the phantom, which is consistent with the simulation results in Fig. 4.

In vivo measurements

Figure 10a shows the fat fraction maps from the middle-calf slice of a healthy volunteer for all three T_1 bias correction/minimization approaches and two water/fat separation approaches. It is difficult to identify any differences in the estimated fat fraction values even in the zoomed view of Fig. 10a due to the strong spatial variation of fat fraction within the muscular regions. Figure 10b shows the flip angle dependence of the estimated fat fraction in an ROI in the medial gastrocnemius, highlighting the significance of the T_1 bias effect (the five presented flip angles data points correspond to the data from the ESFA, ULFA and USFA flip angles). Figure 10c includes a scatter plot of the estimated fat fraction values using all three T_1 bias correction/minimization approaches and two water/fat separation approaches for the 10 repetitions of the *in vivo* experiment. It can be noticed that the USFA approach combined with either the joint fieldmap estimation IDEAL or independent fieldmap estimation IDEAL shows the lowest dispersion of the 10 repetitions of the fat fraction measurements around their mean values, which is consistent with the simulation results (Fig. 4).

DISCUSSION

The correction of the various confounding factors in quantitative water/fat separation can improve the accuracy of the measurement by removing systematic biases, but it can also degrade the noise performance when the complexity of the signal model is increased and more unknowns are introduced. Typical example of degrading the noise properties of the model by increasing the number of unknowns in quantitative water/fat separation is the modeling of T_2* decay as a two T_2* decay instead of a single T_2* decay (26,33,34). The correction of T_1 bias is another example where a trade-off between improving the accuracy and degrading the noise performance must be considered. Specifically, the minimization of the T_1 bias effect on fat fraction measurements derived from chemical/shift based water/fat separation requires the use of small flip angles that lead in general to low SNRs (ESFA approach) (23,25). The correction of the T_1 bias effect on fat quantification measurements requires the acquisition of the IDEAL data at least at two different flip angles, introducing more unknowns and increasing the complexity of the signal model (ULFA approach) (23,25). Instead a novel approach is proposed in this work with the acquisition of the IDEAL data at two small flip angles such that the water signal is assumed to be T_1-independent for the first flip angle and the fat signal is assumed to be T_1-independent for the second flip angle (USFA approach). Although the USFA approach discards the information for the water signal at the second flip angle, the USFA approach benefits from the use of the T_1-independent equations for estimating the water and fat signals. Taking into account the information for the water signal at the second flip angle would require the estimation of T_1 of water and increase the complexity of the model with the potential of degrading the noise performance of the water signal estimation.

The presented simulations, phantom and in vivo results show that the USFA approach can minimize the T_1 bias with improved noise performance over the ESFA and ULFA approaches in tissues with large T_1 difference between water and fat. In the case of tissues

with small T_1 difference between water and fat, the noise efficiency of the ESFA approach is higher than the noise efficiency of ULFA approach (25). Therefore, it should be emphasized that the presented arguments related to the selection of flip angles refer to the case of tissues with large T_1 difference between water and fat. Furthermore, the acquisition of two flip angles as in the ULFA and the USFA approaches or the acquisition of two averages for the same small flip angle as in ESFA approach can be prohibitive in the case of quantitative water/fat separation in body parts where the data acquisition has to be performed within a single breath hold or respiratory gating is required. In that case, the small flip angle approach with a single average will be preferred. However, the present results show that in the case of tissues large T_1 difference between water and fat and where two averages of the same flip angle can be acquired it is preferable to acquire the IDEAL data at two different flip angles (selected as in the USFA approach) than to acquire the IDEAL data at the same flip angle two times (as in the ESFA approach). Similar arguments might be applicable for more than two averages and more than two flip angles, but such an analysis was outside the scope of the present study.

An additional consideration when comparing the different T_1 bias correction/minimization procedures on quantitative chemical shift based water/fat separation is the instability at low and high fat fractions, as previously reported by Liu et al (23). Specifically, the ULFA approach suffers from instabilities due to erroneously estimated T_1 values occurring when the fraction of one of the species (water or fat) is small. The ESFA and the USFA approaches do not suffer from this type of instability, since T_1 estimation is not required to remove the T_1-bias effect in the estimation of the fat fraction (23). In the present work, outlier removal is employed in the analysis of the numerical simulations and averaging over ROIs is employed in the analysis of the phantom and *in vivo* data, reducing the effect of the instabilities in fat fraction estimation with the ULFA approach at low and high fat fractions due to erratic estimates of T_1. However, the instability of the T_1 correction step in the ULFA approach should be always considered when comparing the different T_1 bias correction/ minimization procedures on quantitative chemical shift based water/fat separation.

A further improvement of the noise performance of IDEAL data acquired at multiple flip angles can be achieved by joint estimation of the T_1-weighted water signal, the T_1-weighted fat signal, the fieldmap and T_2* values based on the multi-echo source signals at multiple flip angles. The joint estimation approach, labeled as joint fieldmap estimation IDEAL, has the advantage of improving the noise performance of the estimated water and fat signals relative to the approach of solving the water/fat separation problem at every flip angle separately. This improvement occurs since the approach of joint estimation reduces the total number of unknowns. It should be pointed out that, in the present implementation, fieldmap smoothing is used in solving the independent fieldmap estimation IDEAL problem at every flip angle, as previously proposed (28). The fieldmap values from the solution of the independent fieldmap estimation IDEAL problem at every flip angle are averaged and used as initial guess for solving the joint field map estimation IDEAL problem. There is no additional fieldmap smoothing applied when solving the joint field map estimation IDEAL problem. However, fieldmap smoothing is an operation that can be always performed as an additional regularization during the joint field map estimation IDEAL reconstruction.

The goal of the present work was not to study the T_1 dependence of the water and fat compartments on fat fraction, but its implications should be discussed. Hu et al. (35) have recently reported a strong dependence of the T_1 of the main fat peak with the fat fraction in water/fat mixtures based on single-voxel spectroscopy measurements in oil-water emulsions and pork-kidney lard mixtures. Specifically, in Hu's study (35) the T_1 of the main fat peak approaches the T_1 of water in water/fat mixtures with very low fat fractions (of the order of 10%). This result contradicts with the results of previous *in vivo* studies (36,37) measuring

the T_1 of skeletal muscle metabolites showing a rather constant value for the T_1 of the methylene peak of extramyocellular lipids (of the order of 360 ms). The present phantom results also show a very small change of the T_1 of the main fat peak for the phantom emulsion between 10% and 20% fat fraction. The above differences could be attributed to the observation that the spectra shown in Hu's work are characterized by much broader linewidths than the spectra measured in the present water/fat phantom (38) or the *in vivo* spectra measured routinely in skeletal muscle regions with low fat content. Broad linewidths in MR spectra can affect the peak area calculation and may induce peak area values for the water and fat peaks dependent on the fat fraction. Nevertheless, the issue of the fat fraction dependence of the T_1 of fat could be dependent on the type of fat depot under study and further work in that direction would be necessary.

The presented ESFA, ULFA and ESFA approaches have been designed for T_1 bias correction and minimization in quantitative water/fat separation, but are not suitable, in their current implementation, for T_1 mapping of water and fat. A detailed analysis of the T_1 variation of water and fat compartments with fat fraction would require the addition of a robust absolute flip angle mapping approach to the present ULFA approach (39). However, single voxel spectroscopy experiments confirmed the small variation of the T_1 of the main fat peak both in phantom and previous *in vivo* measurements of the T_1 of the methylene peak of extramyocellular lipids support this hypothesis (36,37). A rather wide range of variation was also selected for the T_{1w} (between 500 ms and 2000 ms) in an effort to take into account the dependence of T_{1w} on muscle fiber composition (40) and to include potentially severely altered T_{1w} values in diseased muscles. Therefore, the variation of the T_{1w} in a given range and the relative constancy of the T_{1f} of the fat are the only constraints for which the presented ESFA and USFA approaches minimize the T_1 bias effect. The implementation of the ULFA approach is not accompanied by any constraint since it exactly corrects for the T_1 effect, although the optimal flip angles selection would obviously depend on the T_1 values of water and fat.

The present work has some limitations. The precalibrated fat spectrum used in the water/fat separation of the *in vivo* data was borrowed from the literature (31). The accuracy of the precalibrated fat spectrum is an important factor that can affect the accuracy of quantitative chemical shift based water/fat separation. Further work would be needed to understand the variation of muscular fat spectrum with fat fraction and muscle region for a given subject and its variation among subjects, including potential variable levels of unsaturated fatty acids. Furthermore, the following confounding factors in the quantitative water/fat separation have not been taken into consideration: eddy currents effects (41), T_2* difference between water and fat compartments (42) and different T_1s for the different fat peaks (38). Regarding the eddy currents compensation, eddy currents induced phase errors can be assessed using a magnitude tuning approach as in (41). The phase contribution from eddy currents was studied in the phantom and found to be not significant. However, the noise performance of the magnitude tuning approach in dual flip angle acquisitions would require further analysis. Regarding the need to model different T_2* for water and fat, the muscle T_2* value is expected to be in the range 24–29 ms at 3 T (43) and the fat T_2* is expected to be close to 26 ms at 3 T (18). Therefore, the single T_2* decay model might be adequate in muscle applications of quantitative water/fat separation. Regarding the difference in T_1 values among the different fat peaks, the effect of different T_1 values for the different fat peaks should be important primarily at high flip angles and high fat fractions. A separate experiment in a vial containing only fat showed that the use of the same T_1 for the different fat peaks in the fat only region lead to an underestimation of the fat fraction by 2–3% relative to the use of different T_1s for the different fat peaks with the ULFA approach.

The present analysis focused on examining the noise performance of different T_1 bias correction/minimization procedures for 3D IDEAL-SPGR data. Chemical shift based water/fat separation methods can use either 2D or 3D sequences. 2D sequences lead to longer in general TR values for the same slice coverage as the 3D sequences and use thus higher flip angles than the 3D sequences (44). The arguments analyzed in the present work can be generalized for the 2D acquisition case. However, it has to be emphasized that 2D sequences at high flip angles will suffer from slice profile effects, which can make the signal behavior deviate from the traditional SPGR signal expression (45,46). Therefore, in the case of strong slice profile effects, the insensitivity of the three T_1 bias correction/minimization approaches to absolute flip angle variations needs to be re-evaluated.

The present analysis optimizes the T_1-correction of fat fraction derived from chemical shift based water/fat separation in the case where the T_1 of fat and water are unknown. Depending on the application, alternative approaches for the T_1-correction procedure could be the *a priori* knowledge of the T_1 values of fat and water or the precalibration of the T_1 value of the fat compartment as in (38). In the case where the T_1 of fat and water are exactly known, Eqs. [4] and [6] could be directly used to remove T_1 effects based on the acquisition of data at a single flip angle. The flip angle that would optimize the noise performance would be between the Ernst flip angle of water and the Ernst flip angle of fat depending on the fat fraction. However, when the T_1 values of water and fat are *a priori* known, attention should be paid on the effect of the absolute flip angle variations on the T_1 correction step. Furthermore, in the case where the T_1 of fat is precalibrated, the ULFA approach could be used. However, when the T_1 value of fat is known and is used to reduce the number of unknowns in the T_1-correction step, the insensitivity of the ULFA approach to absolute flip angle variations (as shown in Appendix A2) does not hold. Therefore, the effect of absolute flip variations due to both transmit B_1 inhomogeneities and RF calibration errors (39) should be taken into consideration on the T_1-correction procedure when the T_1 values of fat and water are a priori known or when the T_1 value of the fat is precalibrated.

Finally, the present work focused on the application of chemical shift based fat quantification methods on the skeletal muscle, which would be important in the context of metabolic syndrome (including obesity and diabetes) (1,2) as well as in the context of muscle dystrophies (20). However, the conclusions of this analysis can be generalized in the case of other tissues with large T_1 differences between water and fat compartments. Fat quantification in the breast (47) and the red bone marrow (48,49) are potential applications where the findings of the present work could be applied.

CONCLUSION

Novel approaches for T_1 bias effect correction and minimization in quantitative chemical shift based water/fat separation have been introduced and compared with previously proposed approaches. Simulations, phantom and *in vivo* measurements have been employed in order to characterize the noise performance of different fat fraction T_1 bias correction/minimization approaches. A novel approach, labeled as the unequal small flip angle approach, is proposed for the minimization of the T_1 bias effect. The results show that the use of two small unequal flip angles, selected such the water signal is assumed to be T_1-independent for the first flip angle and the fat signal is assumed to be T_1-independent for the second flip angle, has superior noise performance to the use of the same small flip angle twice (no T_1 estimation required) and the use of two unequal large flip angles (T_1 estimation required). It is also shown that a novel approach performing a joint water/fat separation at the two employed flip angles can improve further the noise performance relative to the traditional approach of performing the water/fat separation separately at every flip angle.

Acknowledgments

This research is supported by NIH R01-AG17762. The authors would like to thank Joseph Schooler for help with the phantom construction and Diego Hernando for useful discussion.

APPENDIX A1: Matrix formulation of dual flip angle IDEAL

With the signals collected at six echoes and two flip angles, Eq. [3] can be formatted in the following matrix form:

$$\mathbf{S}=\mathbf{P}(\psi)\cdot\mathbf{A}\cdot\mathbf{T}\cdot\mathbf{M} \quad [13]$$

where

$$\mathbf{P}(\psi)=\begin{pmatrix} \exp(j2\pi\psi t_1) & \dots & 0 & \exp(j2\pi\psi t_1) & \dots & 0 \\ \dots & \dots & \dots & \dots & \dots & \dots \\ 0 & 0 & \exp(j2\pi\psi t_6) & 0 & 0 & \exp(j2\pi\psi t_6) \end{pmatrix} \quad [14]$$

$$\mathbf{A}=\begin{pmatrix} 1 & \sum_{p=1}^{P} a_{p,cor}(\alpha_1)\exp(j2\pi\Delta f_p t_1) & 0 & 0 \\ \dots & \dots & \dots & \dots \\ 1 & \sum_{p=1}^{P} a_{p,cor}(\alpha_1)\exp(j2\pi\Delta f_p t_6) & 0 & 0 \\ 0 & 0 & 1 & \sum_{p=1}^{P} a_{p,cor}(\alpha_2)\exp(j2\pi\Delta f_p t_1) \\ \dots & \dots & \dots & \dots \\ 0 & 0 & 1 & \sum_{p=1}^{P} a_{p,cor}(\alpha_2)\exp(j2\pi\Delta f_p t_6) \end{pmatrix} \quad [15]$$

$$\mathbf{S}=\begin{pmatrix} S(t_1,\alpha_1) \\ \dots \\ S(t_6,\alpha_1) \\ S(t_1,\alpha_2) \\ \dots \\ S(t_6,\alpha_2) \end{pmatrix} \quad [16]$$

The matrices **T, M** depend on the employed T_1 bias minimization/correction approach:

For the ESFA approach: $\alpha_1 = \alpha_2 = \alpha$:

$$\mathbf{T}=\begin{pmatrix} 1 & 0 \\ 0 & 1 \\ 1 & 0 \\ 0 & 1 \end{pmatrix}, \mathbf{M}=\begin{pmatrix} M_w(\alpha) \\ M_f(\alpha) \end{pmatrix} \quad [17]$$

For the ULFA approach:

$$\mathbf{T}=\begin{pmatrix} 1 & 0 & 0 & 0 \\ 0 & 1 & 0 & 0 \\ 0 & 0 & 1 & 0 \\ 0 & 0 & 0 & 1 \end{pmatrix}, \mathbf{M}=\begin{pmatrix} M_w(\alpha_1) \\ M_f(\alpha_1) \\ M_w(\alpha_2) \\ M_f(\alpha_2) \end{pmatrix} \quad [18]$$

For the USFA approach:

$$\mathbf{T}=\begin{pmatrix} 1 & 0 & 0 \\ 0 & 1 & 0 \\ 0 & 0 & 1 \\ 0 & \frac{\alpha_2}{\alpha_1} & 0 \end{pmatrix}, \mathbf{M}=\begin{pmatrix} M_w(\alpha_1) \\ M_f(\alpha_1) \\ M_w(\alpha_2) \end{pmatrix} \quad [19]$$

APPENDIX A2: Insensitivity of ULFA approach to absolute flip angle variations

For small flip angles such that $\sin(\alpha) \approx \alpha$ and $\cos(\alpha) \approx 1 - \alpha^2/2$

$$\rho_i \approx \frac{M_i(\alpha_1)M_w(\alpha_2)\left(\alpha_2^2 - \alpha_1^2\right)}{M_i(\alpha_2)\alpha_1\alpha_2^2 - M_i(\alpha_1)\alpha_2\alpha_1^2} \quad [20]$$

where i=w,f.

In the presence of absolute flip angle variations by a relative factor $\Delta\alpha$ from the nominal flip angles α_{1nom} and α_{2nom}, such that the actual flip angles are $\alpha_1 = \Delta\alpha\ \alpha_{1nom}$ and $\alpha_2 = \Delta\alpha\ \alpha_{2nom}$

$$\rho_i \approx \frac{1}{\Delta\alpha}\frac{M_i(\alpha_1)M_i(\alpha_2)\left(\alpha_{2nom}^2 - \alpha_{2nom}^2\right)}{M_i(\alpha_2)\alpha_{1nom}\alpha_{2nom}^2 - M_i(\alpha_1)\alpha_{2nom}\alpha_{1nom}^2} \quad [21]$$

Therefore $f = \rho_f / (\rho_w + \rho_f)$ becomes independent of $\Delta\alpha$.

REFERENCES

1. Gallagher D, Kuznia P, Heshka S, Albu J, Heymsfield SB, Goodpaster B, Visser M, Harris TB. Adipose tissue in muscle: a novel depot similar in size to visceral adipose tissue. Am J Clin Nutr. 2005; 81(4):903–910. [PubMed: 15817870]
2. Kim J, Heshka S, Gallagher D, Kotler DP, Mayer L, Albu J, Shen W, Freda PU, Heymsfield SB. Intermuscular adipose tissue-free skeletal muscle mass: estimation by dual-energy X-ray absorptiometry in adults. J Appl Physiol. 2004; 97(2):655–660. [PubMed: 15090482]
3. Vettor R, Milan G, Franzin C, Sanna M, De Coppi P, Rizzuto R, Federspil G. The origin of intermuscular adipose tissue and its pathophysiological implications. Am J Physiol Endocrinol Metab. 2009 in press.
4. Boesch C, Machann J, Vermathen P, Schick F. Role of proton MR for the study of muscle lipid metabolism. NMR Biomed. 2006; 19(7):968–988. [PubMed: 17075965]
5. Boesch C, Slotboom J, Hoppeler H, Kreis R. *In vivo* determination of intra-myocellular lipids in human muscle by means of localized 1H-MR-spectroscopy. Magn Reson Med. 1997; 37(4):484–493. [PubMed: 9094069]

6. Schick F, Eismann B, Jung WI, Bongers H, Bunse M, Lutz O. Comparison of localized proton NMR signals of skeletal muscle and fat tissue *in vivo*: two lipid compartments in muscle tissue. Magn Reson Med. 1993; 29(2):158–167. [PubMed: 8429779]
7. Schick F, Machann J, Brechtel K, Strempfer A, Klumpp B, Stein DT, Jacob S. MRI of muscular fat. Magn Reson Med. 2002; 47(4):720–727. [PubMed: 11948733]
8. Boettcher M, Machann J, Stefan N, Thamer C, Haring HU, Claussen CD, Fritsche A, Schick F. Intermuscular adipose tissue (IMAT): association with other adipose tissue compartments and insulin sensitivity. J Magn Reson Imaging. 2009; 29(6):1340–1345. [PubMed: 19422021]
9. Positano V, Christiansen T, Santarelli MF, Ringgaard S, Landini L, Gastaldelli A. Accurate segmentation of subcutaneous and intermuscular adipose tissue from MR images of the thigh. J Magn Reson Imaging. 2009; 29(3):677–684. [PubMed: 19243051]
10. Goodpaster BH, Stenger VA, Boada F, McKolanis T, Davis D, Ross R, Kelley DE. Skeletal muscle lipid concentration quantified by magnetic resonance imaging. Am J Clin Nutr. 2004; 79(5):748–754. [PubMed: 15113711]
11. Weis J, Courivaud F, Hansen MS, Johansson L, Ribe LR, Ahlstrom H. Lipid content in the musculature of the lower leg: evaluation with high-resolution spectroscopic imaging. Magn Reson Med. 2005; 54(1):152–158. [PubMed: 15968653]
12. Weis J, Johansson L, Courivaud F, Karlsson FA, Ahlstrom H. Quantification of intramyocellular lipids in obese subjects using spectroscopic imaging with high spatial resolution. Magn Reson Med. 2007; 57(1):22–28. [PubMed: 17152088]
13. Weis J, Johansson L, Ortiz-Nieto F, Ahlstrom H. Assessment of lipids in skeletal muscle by high-resolution spectroscopic imaging using fat as the internal standard: comparison with water referenced spectroscopy. Magn Reson Med. 2008; 59(6):1259–1265. [PubMed: 18421681]
14. Glover GH, Schneider E. Three-point Dixon technique for true water/fat decomposition with B_0 inhomogeneity correction. Magn Reson Med. 1991; 18(2):371–383. [PubMed: 2046518]
15. Ma J. Dixon techniques for water and fat imaging. J Magn Reson Imaging. 2008; 28(3):543–558. [PubMed: 18777528]
16. Reeder SB, Wen Z, Yu H, Pineda AR, Gold GE, Markl M, Pelc NJ. Multicoil Dixon chemical species separation with an iterative least-squares estimation method. Magn Reson Med. 2004; 51(1):35–45. [PubMed: 14705043]
17. Bydder M, Yokoo T, Hamilton G, Middleton MS, Chavez AD, Schwimmer JB, Lavine JE, Sirlin CB. Relaxation effects in the quantification of fat using gradient echo imaging. Magn Reson Imaging. 2008; 26(3):347–359. [PubMed: 18093781]
18. Yu H, Shimakawa A, McKenzie CA, Brodsky E, Brittain JH, Reeder SB. Multiecho water-fat separation and simultaneous R_2* estimation with multifrequency fat spectrum modeling. Magn Reson Med. 2008; 60(5):1122–1134. [PubMed: 18956464]
19. Reeder SB, Pineda AR, Wen Z, Shimakawa A, Yu H, Brittain JH, Gold GE, Beaulieu CH, Pelc NJ. Iterative decomposition of water and fat with echo asymmetry and least-squares estimation (IDEAL): application with fast spin-echo imaging. Magn Reson Med. 2005; 54(3):636–644. [PubMed: 16092103]
20. Hollingsworth, K.; Willis, T.; Coombs, A.; Mayhew, A.; Eagle, M.; Blamire, A.; Straub, V. Muscle fat infiltration in limb girdle muscular dystrophy 2I: a comparison of qualitative T_{1w} and quantitative Dixon imaging. Proceedings of the 18th Annual Meeting of ISMRM; Stockholm, Sweden. 2010. p. 853
21. Wren TA, Bluml S, Tseng-Ong L, Gilsanz V. Three-point technique of fat quantification of muscle tissue as a marker of disease progression in Duchenne muscular dystrophy: preliminary study. AJR Am J Roentgenol. 2008; 190(1):W8–W12. [PubMed: 18094282]
22. Yu H, McKenzie CA, Shimakawa A, Vu AT, Brau AC, Beatty PJ, Pineda AR, Brittain JH, Reeder SB. Multiecho reconstruction for simultaneous water-fat decomposition and T_2* estimation. J Magn Reson Imaging. 2007; 26(4):1153–1161. [PubMed: 17896369]
23. Liu CY, McKenzie CA, Yu H, Brittain JH, Reeder SB. Fat quantification with IDEAL gradient echo imaging: correction of bias from T_1 and noise. Magn Reson Med. 2007; 58(2):354–364. [PubMed: 17654578]

24. Hu HH, Nayak KS. Quantification of absolute fat mass using an adipose tissue reference signal model. J Magn Reson Imaging. 2008; 28(6):1483–1491. [PubMed: 19025936]
25. Wiens, CN.; Addeman, BT.; Kisch, SJ.; Hines, CD.; Yu, H.; Brittain, JH.; Reeder, SB.; McKenzie, CA. Quantification of noise efficiency with T_1 corrected IDEAL spoiled gradient echo imaging. Proceedings of the 17th Annual Meeting of ISMRM; Honolulu, Hawaii. 2009. p. 4449
26. Hernando D, Liang Z-P, Kellman P. Chemical shift-based water/fat separation: a comparison of signal models. Magn Reson Med. 2010; 64:811–822. [PubMed: 20593375]
27. Hines CD, Yu H, Shimakawa A, McKenzie CA, Brittain JH, Reeder SB. T_1 independent, T_2* corrected MRI with accurate spectral modeling for quantification of fat: validation in a fat-water-SPIO phantom. J Magn Reson Imaging. 2009; 30(5):1215–1222. [PubMed: 19856457]
28. Yu H, Reeder SB, Shimakawa A, Brittain JH, Pelc NJ. Field map estimation with a region growing scheme for iterative 3-point water-fat decomposition. Magn Reson Med. 2005; 54(4):1032–1039. [PubMed: 16142718]
29. Hines, CD.; Yokoo, T.; Bydder, M.; Sirlin, CB.; Reeder, SB. Optimization of flip angle to allow tradeoffs in T_1 bias and SNR performance for fat quantification. Proceedings of the 18th Annual Meeting of ISMRM; Stockholm, Sweden. 2010. p. 2927
30. Reeder, SB.; Hines, CD.; Yu, H.; McKenzie, CA.; Brittain, JH. On the definition of fat-fraction for *in vivo* fat quantification with magnetic resonance imaging. Proceedings of the 17th Annual Meeting of ISMRM; Honolulu, Hawaii. 2009. p. 211
31. Middleton, MS.; Hamilton, G.; Bydder, M.; Sirlin, CB. How much fat is under the water peak in liver fat MR spectroscopy?. Proceedings of the 17th Annual Meeting of ISMRM; Honolulu, Hawaii. 2009. p. 4331
32. Reeder SB, McKenzie CA, Pineda AR, Yu H, Shimakawa A, Brau AC, Hargreaves BA, Gold GE, Brittain JH. Water-fat separation with IDEAL gradient-echo imaging. J Magn Reson Imaging. 2007; 25(3):644–652. [PubMed: 17326087]
33. Bydder M, Shiehmorteza M, Yokoo T, Sugay S, Middleton MS, Girard O, Schroeder ME, Wolfson T, Gamst A, Sirlin C. Assessment of liver fat quantification in the presence of iron. Magn Reson Imaging. 2010; 28(6):767–776. [PubMed: 20409663]
34. Chebrolu, V.; Yu, H.; Pineda, AR.; McKenzie, CA.; Brittain, JH.; Reeder, SB. Noise analysis for chemical shift based water-fat separation with independent T_2* correction for water and fat. Stockholm, Sweden: 2010. p. 2908
35. Hu HH, Nayak KS. Change in the proton T_1 of water and water in mixture. Magn Reson Med. 2010; 63:494–501. [PubMed: 19918888]
36. Krssak M, Mlynarik V, Meyerspeer M, Moser E, Roden M. 1H NMR relaxation times of skeletal muscle metabolites at 3 T. MAGMA. 2004; 16(4):155–159. [PubMed: 15042412]
37. Wang L, Salibi N, Wu Y, Schweitzer ME, Regatte RR. Relaxation times of skeletal muscle metabolites at 7T. J Magn Reson Imaging. 2009; 29(6):1457–1464. [PubMed: 19472422]
38. Karampinos, DC.; Yu, H.; Shimakawa, A.; Souza, RB.; Link, TM.; Li, X.; Majumdar, S. T_1-corrected multi-peak T_2* IDEAL for the quantification of intermuscular adipose tissue. Proceedings of the 18th Annual Meeting of ISMRM; Stockholm, Sweden. 2010. p. 418
39. Wang J, Qiu M, Kim H, Constable RT. T_1 measurements incorporating flip angle calibration and correction *in vivo*. J Magn Reson. 2006; 182(2):283–292. [PubMed: 16875852]
40. Houmard JA, Smith R, Jendrasiak GL. Relationship between MRI relaxation time and muscle fiber composition. J Appl Physiol. 1995; 78(3):807–809. [PubMed: 7775322]
41. Yu, H.; Shimakawa, A.; Reeder, SB.; McKenzie, CA.; Brittain, JH. Magnitude fitting following phase sensitive water-fat separation to remove effects of phase errors. Proceedings of the 17th Annual Meeting of ISMRM; Honolulu, Hawaii. 2009. p. 461
42. Chebrolu V, Hines CD, Yu H, Pineda AR, Shimakawa A, McKenzie CA, Samsonov A, Brittain JH, Reeder SB. Inpendent estimation of T_2* for water and fat for improved accuracy of fat quantification. Magn Reson Med. 2010; 63:849–857. [PubMed: 20373385]
43. Schwenzer NF, Martirosian P, Machann J, Schraml C, Steidle G, Claussen CD, Schick F. Aging effects on human calf muscle properties assessed by MRI at 3 Tesla. J Magn Reson Imaging. 2009; 29(6):1346–1354. [PubMed: 19472391]

44. Wokke, B.; Bos, C.; Eggers, H.; Webb, A.; Kan, H. Feasibility and reproducibility of MR fat-fraction measurements in muscle using iterative signal decomposition with a multifrequency fat signal model. Proceedings of the 18th Annual Meeting of ISMRM; Stockholm, Sweden. 2010. p. 851

45. Brookes JA, Redpath TW, Gilbert FJ, Murray AD, Staff RT. Accuracy o f T_1 measurement in dynamic contrast-enhanced breast MRI using two- and three-dimensional variable flip angle fast low-angle shot. J Magn Reson Imaging. 1999; 9(2):163–171. [PubMed: 10077009]

46. Parker GJ, Barker GJ, Tofts PS. Accurate multislice gradient echo T_1 measurement in the presence of non-ideal RF pulse shape and RF field nonuniformity. Magn Reson Med. 2001; 45(5):838–845. [PubMed: 11323810]

47. Rakow-Penner R, Daniel B, Yu H, Sawyer-Glover A, Glover GH. Relaxation times of breast tissue at 1.5T and 3T measured using IDEAL. J Magn Reson Imaging. 2006; 23(1):87–91. [PubMed: 16315211]

48. Bydder, M.; Liang, H.; Yu, H.; Shimakawa, A.; Brittain, JH.; Bydder, G.; Mell, L. Monitoring bone marrow changes during chemotherapy using MRI fat quantification. Proceedings of the 18th Annual Meeting of ISMRM; Stockholm, Sweden. 2010. p. 2822

49. Karampinos, DC.; Yu, H.; Shimakawa, A.; Han, E.; Link, TM.; Majumdar, S.; Krug, R. Bone marrow fat fraction mapping in the proximal femur *in vivo* using IDEAL gradient echo imaging. Proceedings of the 18th Annual Meeting of ISMRM; Stockholm, Sweden. 2010. p. 791

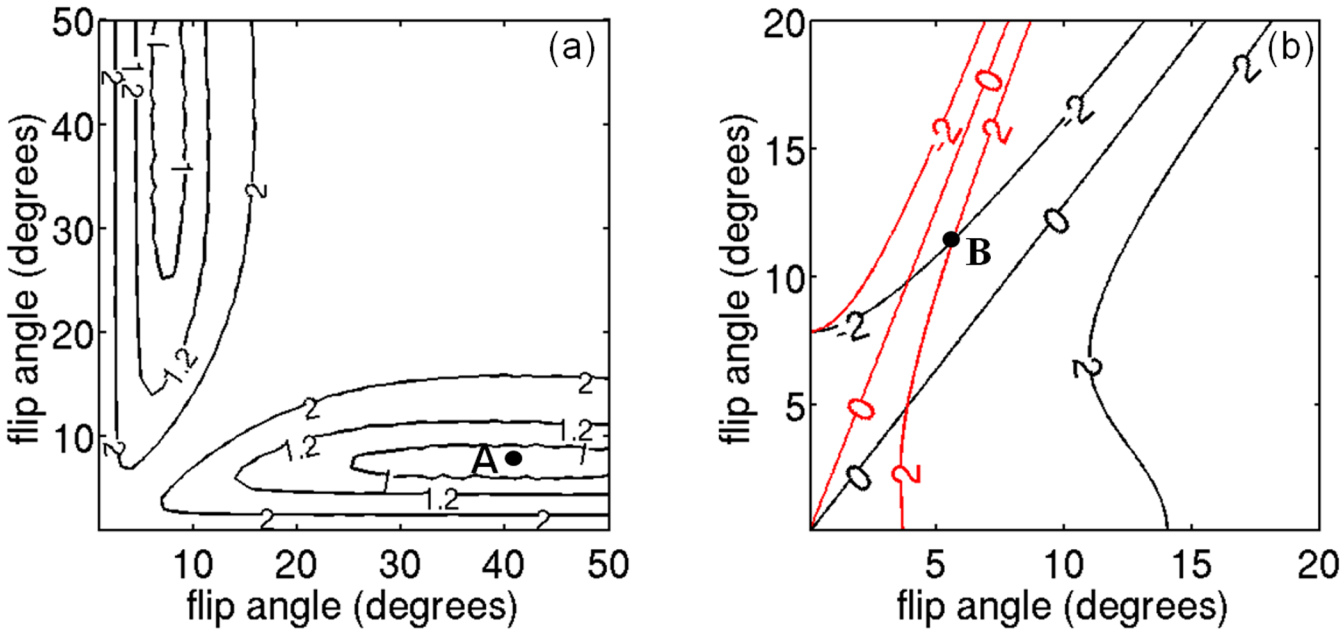

Figure 1.

Design criteria for selection of flip angles in ULFA and USFA approaches. (a) ULFA approach: isocontour lines of mean variance of fat fraction for ULFA approach (values in arbitrary units). The selected flip angles (Point A) correspond to the flip angles that maximize noise performance. (b) USFA approach: isocontour lines of fat fraction bias at 50% fat fraction for $T_{1w}=T_{1wmin}$ (black lines) and $T_{1w}=T_{1wmax}$ (red lines) (values in %). The selected flip angles (Point B) correspond to the flip angles that minimize fat fraction bias over the range of T_{1w}.

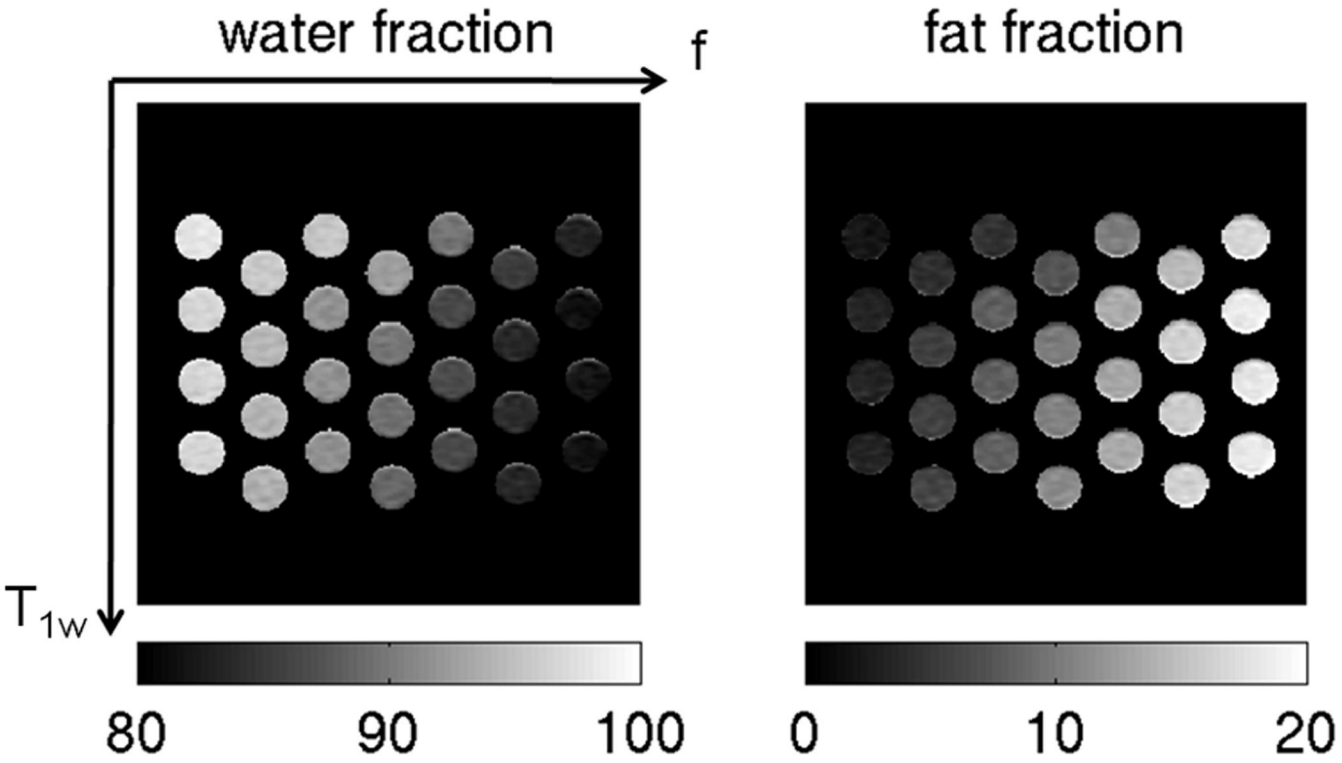

Figure 2.
Water fraction and fat fraction maps in the phantom with the ESFA approach flip angle (3.7°). The fat fraction increases from left to right and the T_1 of water increases from the top to the bottom (values of water and fat fraction are in %).

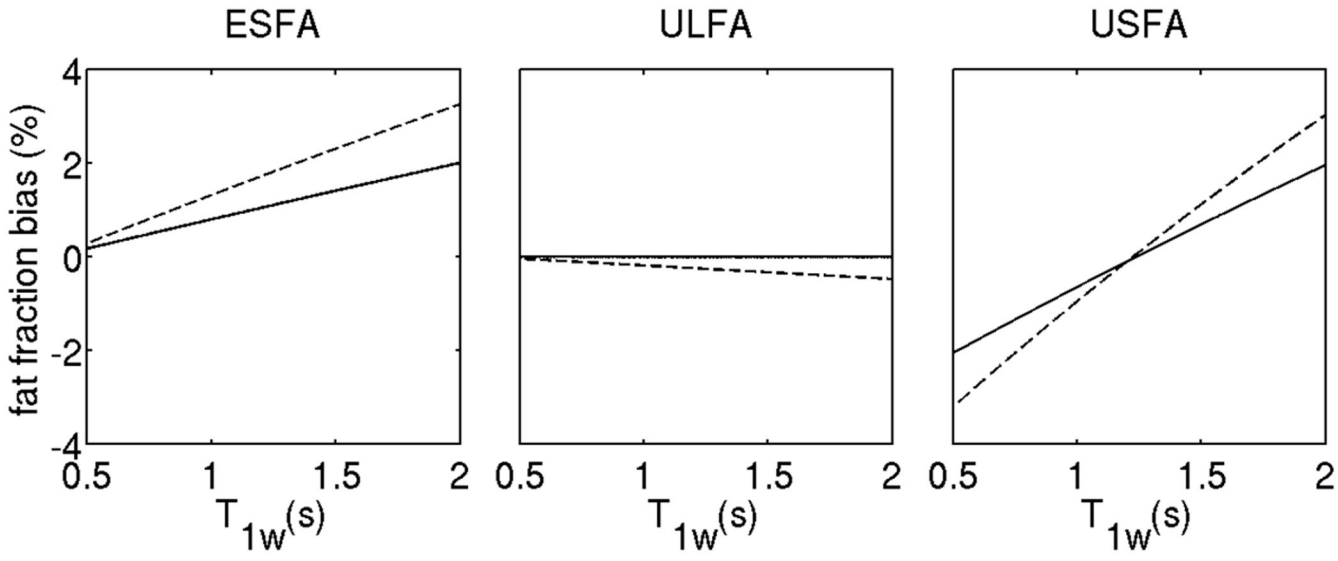

Figure 3.

Sensitivity of fat fraction estimates to absolute flip angle variations: plot of fat fraction bias at 50% fat fraction for the 3 employed T_1-correction approaches as a function of T_{1w} with no absolute flip angle variation (solid line) and with absolute flip angle variation such that the actual flip angle is 30% higher than the nominal flip angle (dashed line).

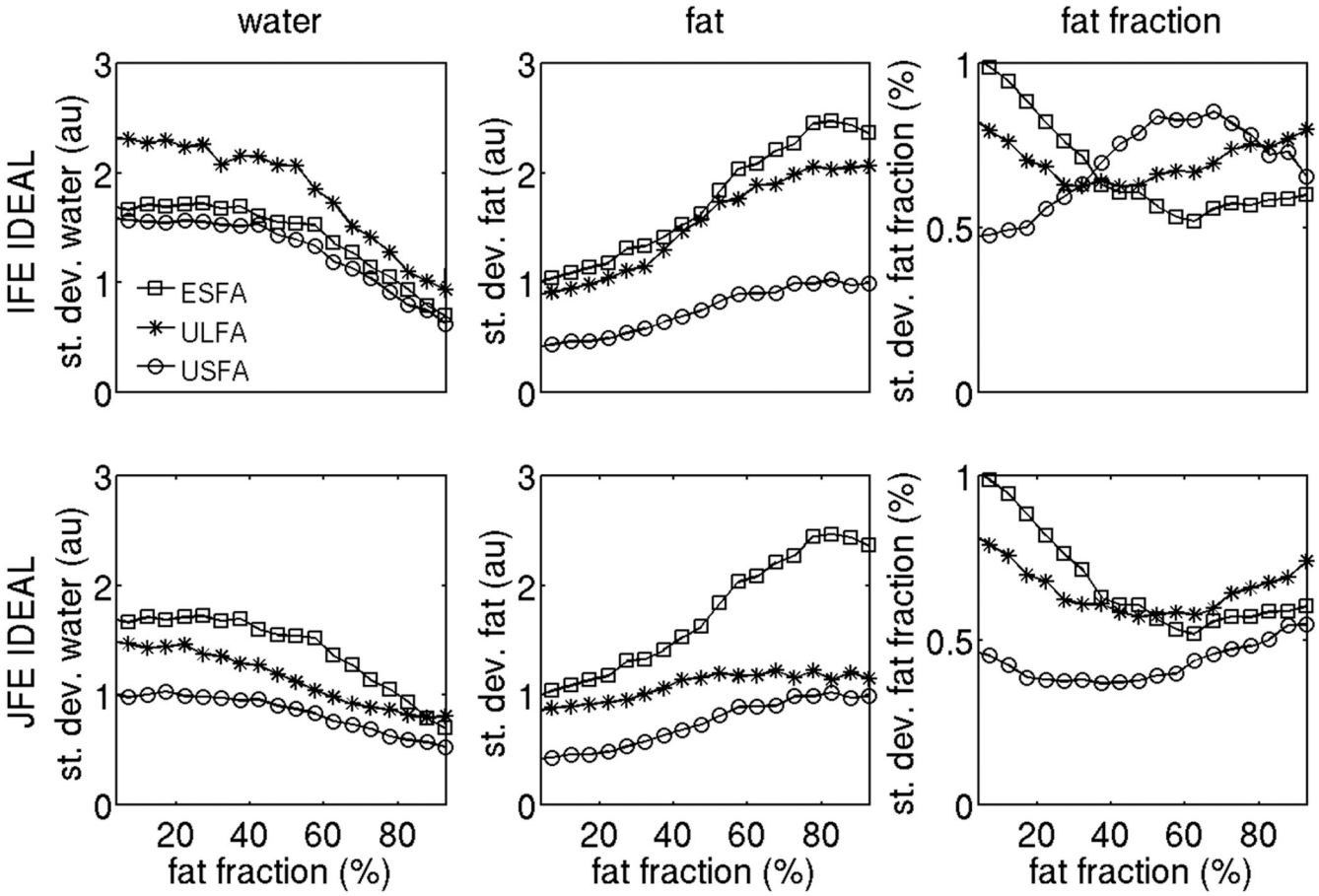

Figure 4.

Noise performance of proton density weighted water signal, proton density weighted fat signal and fat fraction using the 6 options under study on the simulated data. The squares correspond to ESFA approach results, the stars correspond to ULFA approach results and the circles correspond to USFA approach results. The first row shows independent fieldmap estimation IDEAL results and second column shows joint fieldmap estimation IDEAL results.

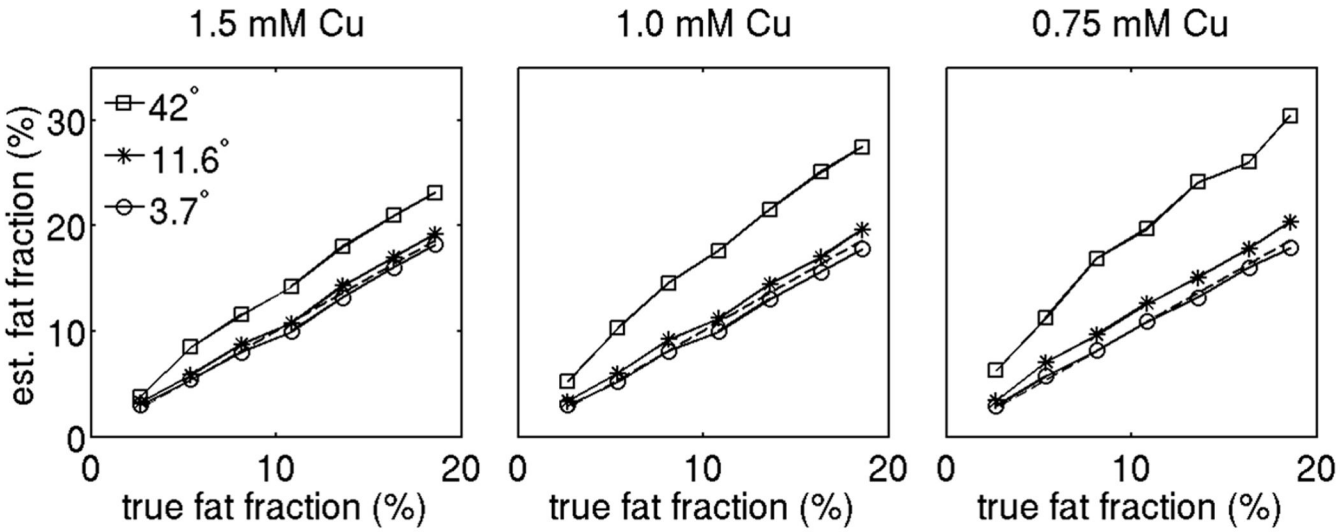

Figure 5.

T_1 bias effect on phantom fat fraction values for different flip angles without any T_1 correction. The squares, stars and circles correspond to the uncorrected fat fraction values with flip angles 42°, 11.6° and 3.7° respectively. The dashed line corresponds to the nominal fat fraction values (identity line).

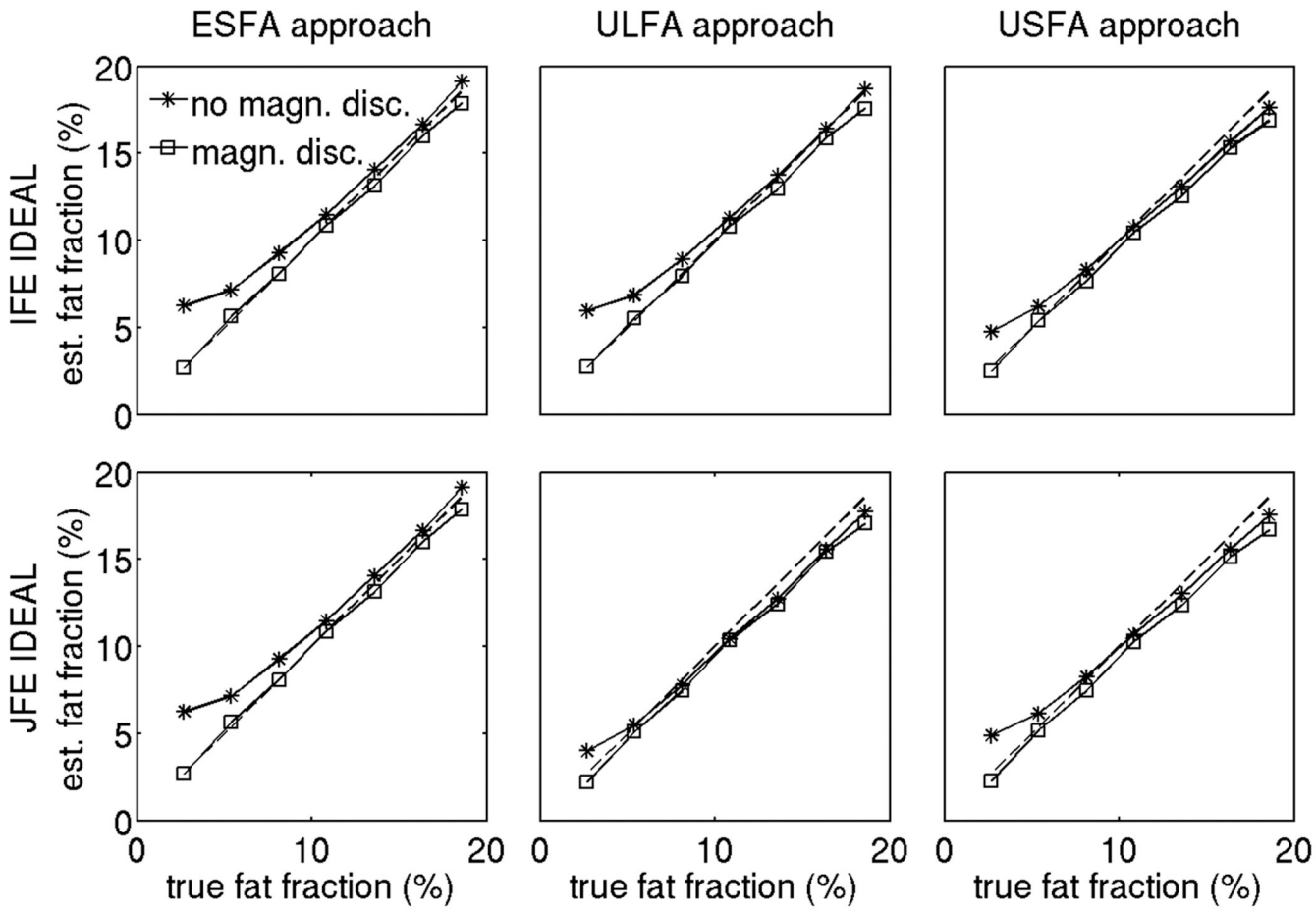

Figure 6.

Noise bias effect on fat fraction of phantom vials with 0.75 mM concentration in Cu for all 6 options under study. The stars show the results without applying the magnitude discrimination approach, the squares show the results with applying the magnitude discrimination approach, and the dashed line shows the nominal fat fraction values (identity line).

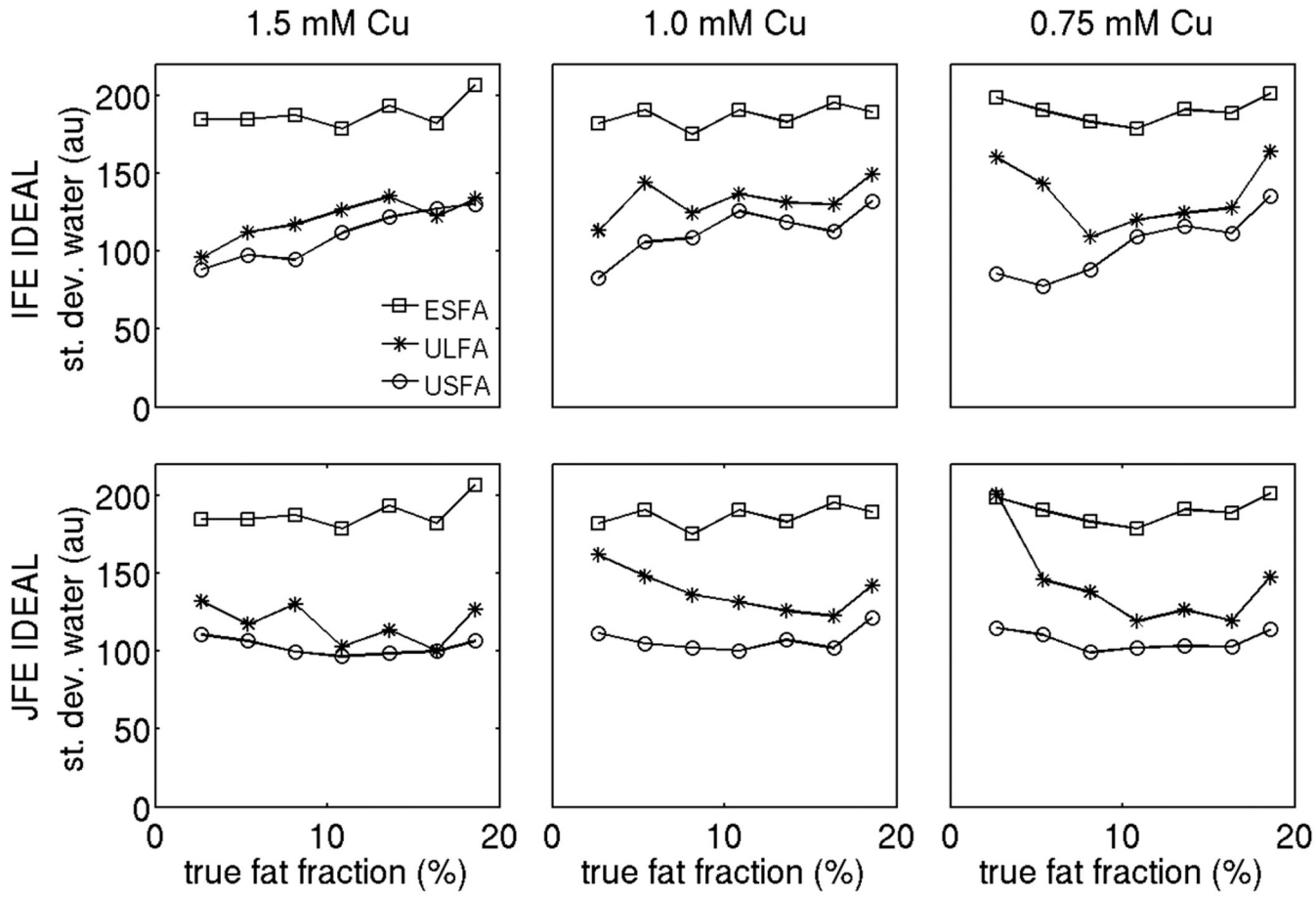

Figure 7.

Comparison of standard deviation of the proton density weighted water signal using the 6 options under study on the phantom data (for three different concentrations in Cu). The squares correspond to ESFA approach results, the stars correspond to ULFA approach results and the circles correspond to USFA approach results. The first row shows independent fieldmap estimation IDEAL results and second column shows joint fieldmap estimation IDEAL results.

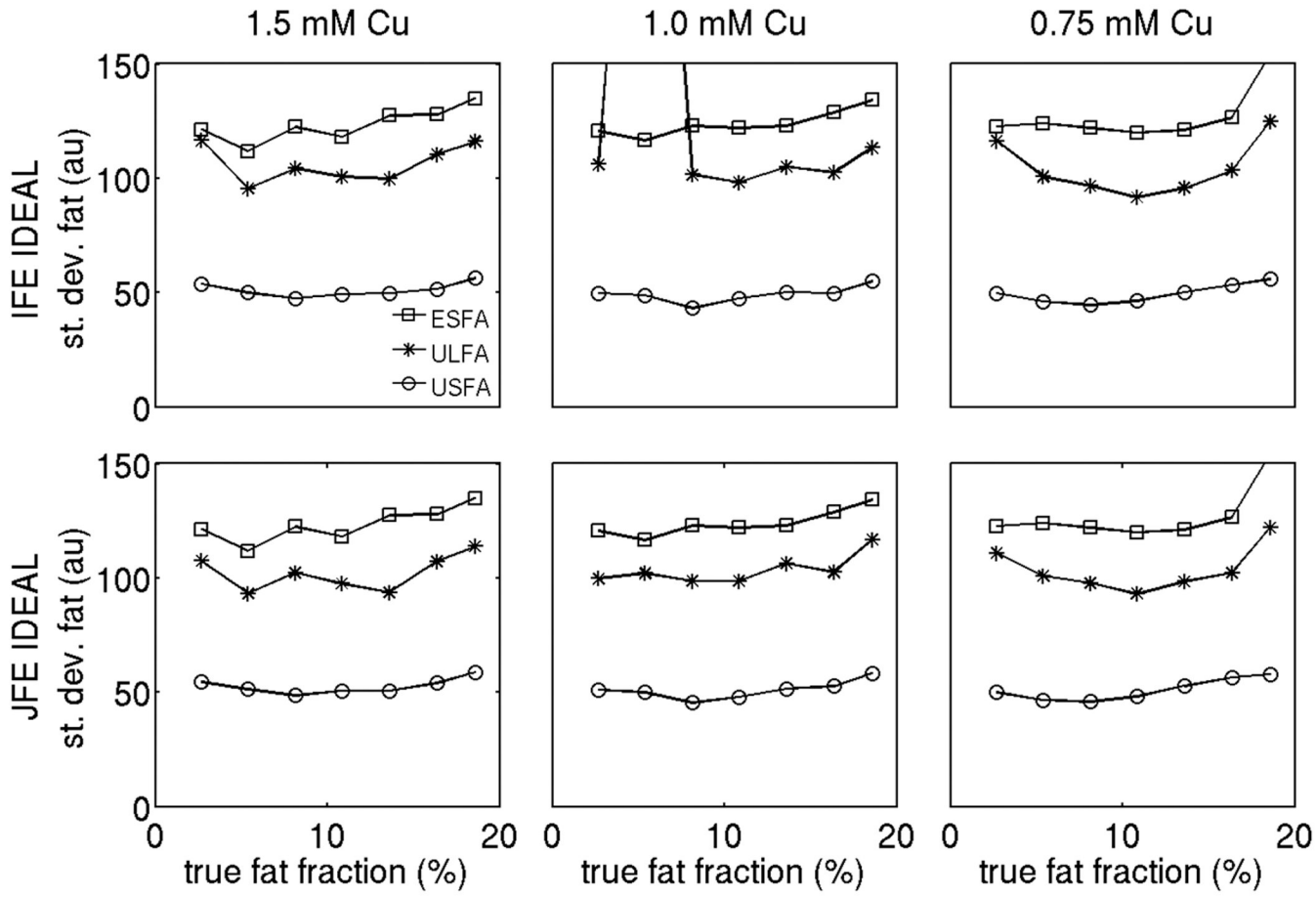

Figure 8.

Comparison of standard deviation of the proton density weighted fat signal using the 6 options under study on the phantom data (for three different concentrations in Cu). The squares correspond to ESFA approach results, the stars correspond to ULFA approach results and the circles correspond to USFA approach results. The first row shows independent fieldmap estimation IDEAL results and second column shows joint fieldmap estimation IDEAL results.

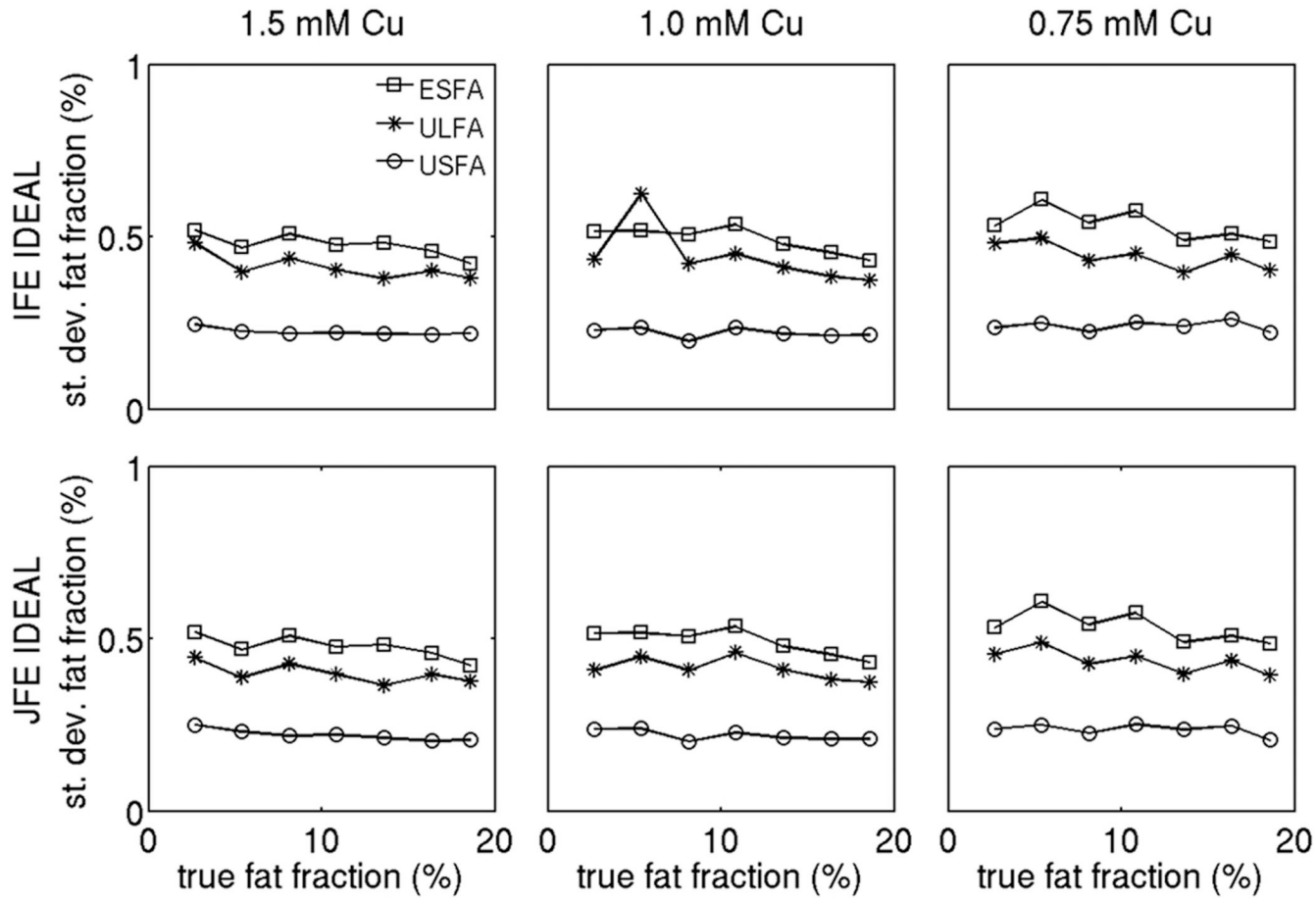

Figure 9.

Comparison of standard deviation of fat fraction using the 6 options under study on the phantom data (for three different concentrations in Cu). The squares correspond to ESFA approach results, the stars correspond to ULFA approach results and the circles correspond to USFA approach results. The first row shows independent fieldmap estimation IDEAL results and second column shows joint fieldmap estimation IDEAL results.

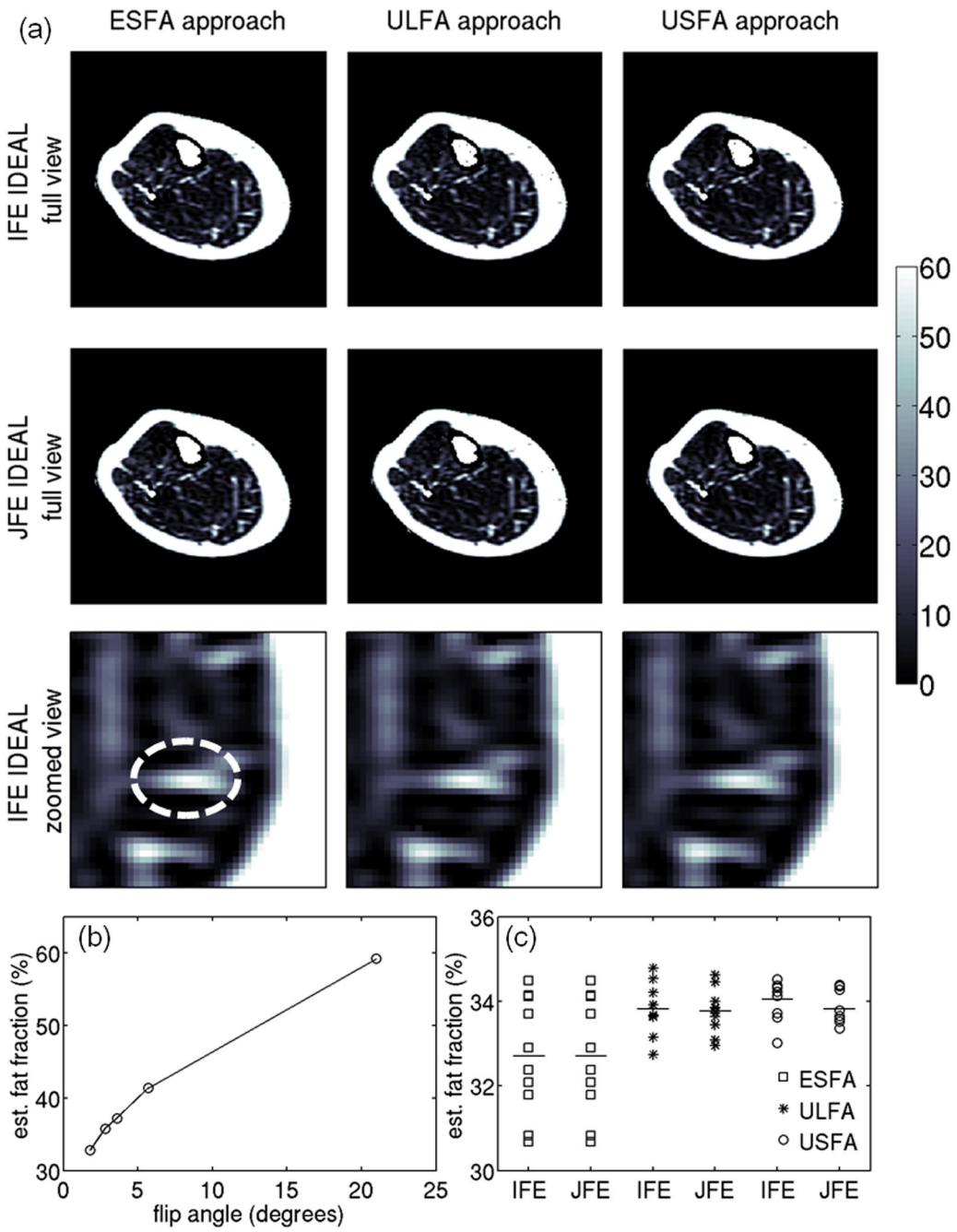

Figure 10.

In vivo results. (a) Fat fraction maps using the 6 options under study (values in %). First two rows show the fat fraction maps for the full FOV and the third row shows the fat fraction maps for a zoomed region in the medial gastrocnemius muscle. (b) Dependence of uncorrected mean fat fraction over the shown ROI with the employed flip angle. (c) Scatter plot of the corrected mean fat fraction over the shown ROI using the 6 options under study for the 10 repetitions of the *in vivo* experiment. The squares correspond to results of the ESFA approach, the stars correspond to results of the ULFA approach and the circles correspond to results of the USFA approach.